

S. Schaefer, S. Albrecht, D. Neher, T. F. Schulze, E. Conrad, L. Korte, B. Rech, J. Würdenweber, A. Gordijn, U. Scherf, and I. Dumsch

Electric Field Distribution in Hybrid Solar Cells Comprising an Organic Donor Polymer and Amorphous Silicon

Abstract: We present a study on the performance and analysis of hybrid solar cells comprising a planar heterojunction between a conjugated donor polymer, P3HT or PCPDTBT, and hydrogenated amorphous silicon (a-Si:H). A comparison of the modeled absorption spectra of the layer stack with the measured external quantum efficiency is used to investigate the contribution of the inorganic and organic material to the photocurrent generation in the device. Although both materials contribute to the photocurrent, the devices exhibit poor quantum efficiencies and low short circuit currents. Bandstructure simulations of the hybrid layer structure reveal that an unfavorable electric field distribution within the planar multilayer structure limits the performance. Using electroabsorption measurements we can show that the electric field is extremely weak in the amorphous silicon but strong in the organic material. The situation changes drastically when the conjugated polymer is p-doped. Doping not only increases the conductivity of the organic material, but also restores the electric field in the amorphous silicon layer. Optimized hybrid solar cells comprising thin doped P3HT layers exhibit energy conversion efficiencies (ECE) up to 2.8 %.

S. Schaefer, S. Albrecht, D. Neher: Universität Potsdam, Institute of Physics and Astronomy, Soft Matter Physics, D-14476 Potsdam, Germany

T. F. Schulze, E. Conrad, L. Korte, B. Rech: Department of Silicon Photovoltaics, Helmholtz Center Berlin for Materials and Energy, Kekulestr. 5, D-12489 Berlin, Germany

J. Würdenweber, A. Gordijn: IEK5-Photovoltaik, Forschungszentrum Jülich, D-52425 Jülich, Germany

U. Scherf, I. Dumsch: Bergische Universität Wuppertal, Macromolecular Chemistry and Institute for Polymer Technology, Gauss-Strasse 20, D-42097 Wuppertal, Germany

1 Introduction

Organic solar cells based on semiconducting molecules and macromolecules improved largely during the last few years, breaking the 10 % efficiency barrier [1]. Many of these polymers absorb strongly in the red part of the spec-

trum, even beyond 750 nm, and can be easily processed from solution. However, most of these devices use soluble fullerene derivatives, which have an only weak absorption in the visible spectral range. Therefore, research has been devoted to alternative acceptor materials. One possibility is the use of inorganic semiconductors. Among these, hydrogenated amorphous silicon is highly promising as it can be processed in efficient thin film photovoltaic devices and it possesses efficient absorption from blue to green, which is complementary to the absorption of some of the low bandgap polymers used in efficient organic photovoltaic devices. Thus, improved efficiency is expected for hybrid devices, which combine amorphous silicon and organic materials in a single hybrid device [2–4]. Seo *et al.* [5] recently published a hybrid tandem cell, with a *pin* a-Si front cell and a low bandgap conjugated polymer blended with a soluble fullerene forming the red-light absorbing back cell. Optimized devices reached PCEs of more than 5.7 %. However, the architecture of such devices is rather complex and comprises up to 8 different layers [6], including a recombination contact between the inorganic and organic subcell. A more simple device structure has been proposed by Gowrishankar *et al.* [3]. Here, a 20 nm thick intrinsic a-Si layer was in direct contact to a 60 nm thick layer of poly(3-hexylthiophene) (P3HT). The concept of this cell was focused on charge generation in the P3HT layer, whereas the amorphous silicon layer contributed less than 10 % to the photocurrent. The efficiency of this device was, however, rather poor. In the same year, P. J. Alet [2] *et al.* presented a (ITO/a-Si:H(n))/a-Si:H(i)/P3HT/Au cell with considerably improved efficiency (PCE = 1.6 %). Chao *et al.* [7] used pentacene to replace the n-doped a-Si layer in a hybrid cell with the structure SnO₂:F/a-Si:H(p,8 nm)/buffer(6 nm)/a-Si:H(i,300 nm)/pentacene(30 nm)/Al and reached up to 3 %. However, the pentacene layer was not used as a photoactive layer in this device but acted as an exciton blocking and charge transport layer. Clearly, there is a large variation of performance data which calls for a more detailed investigation of the limiting processes in these hybrid devices. Here, we report on the analysis and performance of hybrid structures based on *nip*

a-Si:H inverted solar cells where the p-type layer is replaced by either regioregular P3HT or poly(2,6-(4,4-bis-(2-ethylhexyl)-4H-cyclopenta[2,1-b;3,4-b']dithiophene)-alt-4,7(2,1,3-benzothiadiazole)) (PCPDTBT). The layer stack of the hybrid device with MoO₃ as a hole extracting contact is shown in Fig. 1. The concept is believed to facilitate carrier generation in both the amorphous silicon and the polymer layer. Excitons generated in the polymer can be separated at the a-Si:H/P3HT interface to yield free carriers, which is assisted by the large bandoffset between the materials as displayed in the energy diagram in Fig. 1. Light absorption in the intrinsic a-Si:H layer generates free carriers, due to the low exciton binding energies (≈ 100 meV). Note that in this inverted cell structure the electrons will be extracted at the ITO contact, whereas holes have to pass through the entire polymer layer to reach the MoO₃/Al electrode.

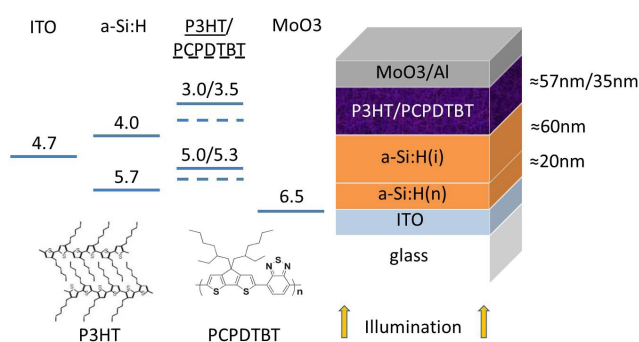


Fig. 1. Energy level diagram and layer stack of the hybrid cell composed of a-Si:H and P3HT or PCPDTBT. In doped hybrid cells, the organic layer contains 5 wt% F4TCNQ. The ionization energies and electron affinities were taken from the literature (a-Si:H [8], P3HT [3], PCPDTBT [9], MoO₃ [10]).

We investigate charge generation and the distribution of electric fields in a-Si:H/organic-hybrid solar cells. A transfer matrix formalism is applied to model the absorption in the hybrid device including interference in the layer stack. The result of this analysis is related to the experimental photoaction spectrum of the hybrid cell with the goal to identify the contributions of the inorganic and organic part of the cell to the photocurrent. Furthermore, the bandstructure of the device is simulated with the Automat for Simulation of Heterostructures program (AFORS-HET) [11] developed for inorganic heterostructure solar cell devices. The results indicate that hybrid cells comprising undoped polymers suffer severely from low electric fields in the intrinsic a-Si:H layer. In order to verify this theoretical prediction we applied electroabsorption (EA) to study the electric field distribution in the device. We show that dop-

ing of the organic layer with the strong acceptor molecule tetrafluorotetracyanoquinodimethane (F4TCNQ) can partially recondition the electric field in the amorphous silicon, leading to much better performance. Following this concept, we realized cells with a thin doped P3HT layer reaching energy conversion efficiencies of up to 2.8 %.

2 Experimental

2.1 Sample preparation

For device preparation, commercial ITO substrates (PGO) were patterned by chemical etching and treated with a hot (60°C) cleaning solution containing 10% of 2-propanol (VLSI Selectipur) in water and using an ultrasonic bath. In a next step ≈ 20 nm phosphorous-doped n-type and ≈ 60 nm intrinsic a-Si:H were deposited by plasma enhanced chemical vapour deposition (PECVD) on top of the ITO. While conventional a-Si:H pin cells have an intrinsic a-Si:H layer thickness of 300 nm to provide sufficient light absorption in the visible range we used i-layers of only 60 nm thickness to allow light entering the device from the a-Si:H side to penetrate up to the polymer layer. For the subsequent organic layer deposition, the sample was transferred to a nitrogen filled glovebox with short intermediate exposure to air for approx. 10 min. In the glovebox P3HT (Merck) was spincoated at 1500 r/min (30 sec) from a chlorobenzene solution with a resulting layer thickness of approximately 60 nm. The doped P3HT layer was spincoated at the same parameters from a mixed solution of P3HT and 5 wt% F4TCNQ in chlorobenzene, where both materials were dissolved and filtered prior to blending. Film thickness remained constant upon introduction of F4TCNQ. One of the cells was completed with a 12 nm p-type layer of a-Si:H and served as a reference cell with a layer structure of ITO/a-Si:H(n,i,p)/MoO₃/Al. Top contacts were realized by physical vapour deposition of ≈ 10 nm MoO₃ and ≈ 100 nm Al at a base pressure of 10^{-6} mbar through shadow masks. The hybrid devices containing PCPDTBT were prepared in the same way as the P3HT devices except that the PCPDTBT thickness was 35 nm. Details of synthesization and preparation of PCPDTBT are published elsewhere [12–15]. Optimized hybrid cells comprised 700 nm thick ZnO:Al and a thin μ c-Si:H layer between ZnO and the n-type a-Si:H layer. Please note that this sample had been exposed to air for a few days before the organic layer was deposited. 20 nm MoO₃ layer coated by 80 nm Au served as the hole-collecting top contact. For the electroabsorption measurements an

ITO/PEDOT:PSS/P3HT/Al reference device was prepared where PEDOT:PSS (Clevios AI 4083) was spin cast in air and subsequently dried in the nitrogen atmosphere of a glove box at 180°C for 10 min.

2.2 Measurements and instrumentation

All experiments were carried out in nitrogen atmosphere. For J-V characteristics a Keithley 2400 source measurement unit was combined with an Oriel class A sun simulator. For the calibration of the sunsimulator to 100 mW/cm² a KG3 filtered silicon reference cell calibrated at Fraunhofer ISE was used. The incident photon to current efficiency (IPCE) was determined by illuminating the sample with monochromatic light from a tungsten lamp (100 W) and a Cornerstone monochromator. A chopper wheel in the light path was used to record the short circuit current with lock-in detection (Princeton Research Systems 5302). The electroabsorption setup used the same light source and monochromator as the IPCE and an Agilent 33120A function generator supplying ac and dc voltage to the sample. The light enters the sample from the ITO side, is reflected at the aluminum back contact and guided to a crystalline silicon diode. The diode signal is preamplified with a Femto DHPA 100 and fed into a lock-in detector (Stanford Research Systems SR 830) referenced to the ac frequency of the function generator. In order to correct the signal from the influence of the lamp spectrum and the silicon diode response function the ER-signal is normalized by a simple reflection spectrum. For this reason the reflection measurement is repeated without voltage applied to the sample and the lock-in is referenced to a chopper wheel placed in the light path. All electroabsorption measurements were carried out under a dc voltage of $V_{dc} = 4$ V in reverse bias and an ac-amplitude of $V_{ac} = 1.5$ V.

2.3 Optical modeling

For the optical modeling of light absorption in the device a transfer matrix formalism [16, 17] was applied, which describes coherent propagation of light, i.e., multiple reflections and interference within the layer stack. The modeling requires the optical constants of each layer, which were taken from the literature only for the metal layer. For the organic and metal oxide layers, reflection and transmission measurements were recorded with a UV-Vis Varian Cary 5000 spectrophotometer equipped with an integrating sphere. Then a Newton-Raphson iterative method was applied to determine the optical constants. For amorphous

silicon the optical constants were determined by ellipsometry.

2.4 Electronic bandstructure simulations

We used the Automat for Simulation of Heterostructures (AFORS-HET) for electronic band-structure simulations of the hybrid layer stack. The simulation developed for amorphous silicon solar cell structures is based on a drift and diffusion approach and applies Poisson's equation to determine the electric potential [11]. The program treats a sequence of semiconductor layers, where a distribution of defect states in the band gap and band tails can be specified. For P3HT, bandtails in the order of the width of the DOS-distribution, $\sigma \approx 100$ meV [18, 19], and a very low defect density of 10^{14} cm⁻³ in the band gap have been chosen. The density of states in the HOMO and LUMO of P3HT was assumed to be 10^{21} cm⁻³. The 5 wt% doped P3HT layer was simulated with a dopant concentration of 5×10^{17} cm⁻³ assuming that not all dopants are ionized [20, 21]. The doping mechanism is assumed to take place via charge transfer from the P3HT HOMO to the low lying LUMO of dopant molecule F4TCNQ leading to free charge carriers in the polymer. We took standard values for Urbach energy and defect distribution of a-Si:H, which were determined by photoelectron yield spectroscopy [22, 23].

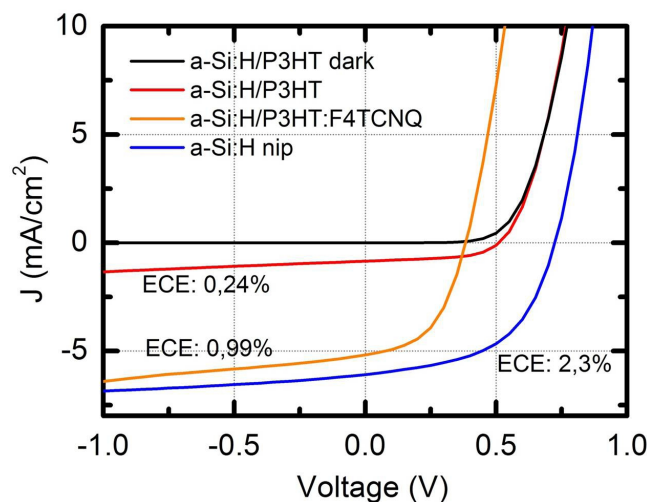


Fig. 2. J-V-characteristics of hybrid solar cells with P3HT and 5 wt% P3HT:F4TCNQ organic layers in comparison to an a-Si:H *nip* reference cell. The reference cell has the same intrinsic a-Si:H layer thickness as the hybrid cells.

Table 1. Solar cell parameters of hybrid cells with P3HT and P3HT:F4TCNQ organic layers compared to an a-Si:H *nip* reference cell with identical intrinsic a-Si:H layer thickness.

material	V_{oc} (V)	J_{sc} ($\frac{mA}{cm^2}$)	η (%)	FF (%)
a-Si:H/P3HT	0.51	0.86	0.24	54.4
a-Si:H/P3HT:F4TCNQ	0.38	5.18	0.99	49.5
a-Si:H <i>nip</i>	0.72	6.09	2.32	52.9

3 Results and Discussion

Fig. 2 compares the J-V-characteristics of a hybrid cell containing ITO/a-Si:H(n,i)/P3HT/MoO₃/Al to the characteristics of the ITO/a-Si:H(nip)/MoO₃/Al reference cell. As reported by others the hybrid cell with a planar interface exhibits a very low efficiency, which is in part attributed to small short-circuit currents. Also, the open circuit voltage of the hybrid device of $V_{oc} = 0.5$ V is significantly lower than in the a-Si:H *nip* reference cell, where values close to $V_{oc} = 0.7$ V were obtained. Interestingly, J_{sc} of the hybrid cell increases strongly upon p-doping of the P3HT layer, reaching current levels comparable to that of the inorganic reference cell. To shine light on these operation limits, we calculated the absorption spectra of the active layers in the hybrid device by using a transfer matrix formalism. The use of a transfer matrix formalism is particularly important when analyzing light absorption in this hybrid stack because the high refractive index contrast between the different materials leads to strong interference effects.

The results of this calculation are illustrated in Fig. 3 in comparison to the quantum efficiency of the hybrid cell. The absorption of intrinsic amorphous silicon layer peaks at 460 nm and exhibits a shoulder at 630 nm, whereas P3HT shows two peaks at 560 nm and 600 nm. For the cell with undoped P3HT, shown in Fig. 3a), the quantum efficiency follows roughly the sum of the absorption spectra of P3HT and a-Si:H, indicating that both materials contribute to the photocurrent according to their fractional absorption. This implies that excitons generated in the polymer are indeed dissociated at the hybrid interface. Furthermore holes generated in amorphous silicon are transferred to the organic layer and leave the device through the metal top contact. Although both processes are active, the hybrid cell with the undoped polymer layer is rather inefficient. In particular, IPCE is largely reduced as compared to the fully inorganic device throughout the a-Si absorption range, meaning that the collection of free charges from the i-a-Si becomes inefficient when replacing p-a-Si by the undoped polymer. Interestingly the same device with a doped P3HT layer exhibits much higher short circuit currents. As

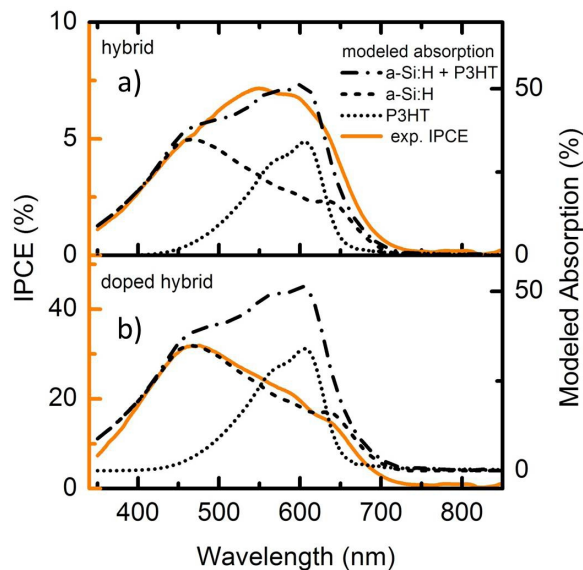


Fig. 3. a) IPCE of the ITO/a-Si:H(n,i)/P3HT/MoO₃/Al device in comparison to the modeled absorption spectrum of the photoactive layers: intrinsic a-Si:H and P3HT as well as the sum of them. The IPCE is similar to the sum of the active layers. b) The IPCE of ITO/a-Si:H(n,i)/P3HT:F4TCNQ/MoO₃/Al device resembles the absorption spectrum of a-Si:H.

shown in Fig. 3b), the inspection of the ipce spectrum reveals a significant increase in the absorption range of the amorphous silicon, while contributions from the organic component are missing in the spectrum. The lack of organic contribution seems intuitive since doping of organic materials is well known to induce defect states that lead to high recombination rates, similar as in amorphous silicon. Since doping also increases the conductivity of P3HT by several orders of magnitude its performance as hole transport layer is strongly enhanced. Consequently it seems that the low conductivity of the undoped organic material limits the device performance. However fully organic P3HT/PCBM solar cells exhibit high short circuit currents in the order of 11-12 mA/cm² which proves the ability of the polymer to conduct relatively high currents also without doping [6]. Alternatively the weak performance of the undoped hybrid cell might have another origin, namely an unfavorable electric field distribution within the device for two reasons:

1. In general the potential drop across the intrinsic a-Si:H layer in a pin cell is due to the different Fermi-level positions in n and p type materials, whereas in the doped a-Si:H layers the bands are almost flat. Inserting an undoped organic layer leads to a potential drop also in the organic layer and thereby reduces the field in the intrinsic a-Si:H layer.

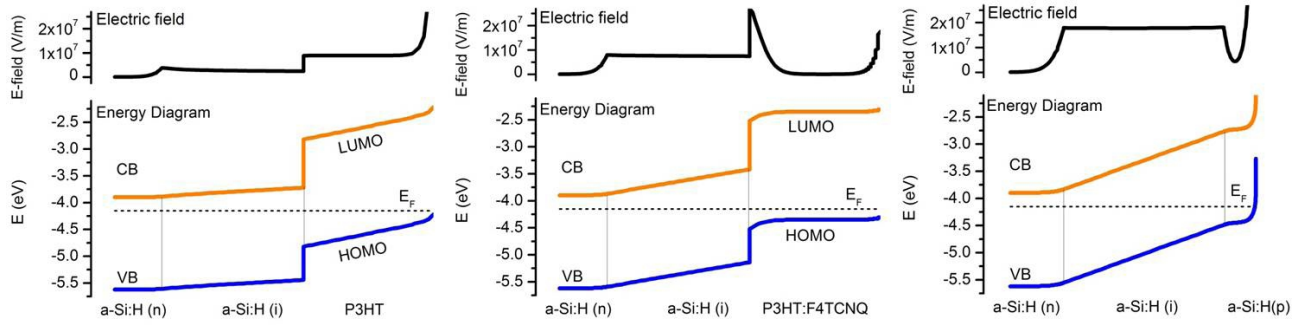


Fig. 4. Electronic band structure simulation of left panel: ITO/a-Si:H(n,i)/P3HT/MoO₃/Al, center panel: ITO/a-Si:H(n,i)/P3HT:F4TCNQ/MoO₃/Al, right panel: ITO/a-Si:H(nip)/MoO₃/Al. The top graphs show the electric field distribution in the different layer systems

2. Inorganic a-Si:H pin cells are homojunctions and no band-offsets arise between the subsequent layers. On the other hand, we cannot exclude the presence of interfacial dipoles at the a-Si/P3HT interface, which can potentially lower the field within the intrinsic a-Si layer.

Figure 4 shows the results of electronic band structure simulations with the simulation tool AFORS-HET. The calculations for the hybrid device with an undoped P3HT layer show a rather low potential drop across the intrinsic amorphous silicon, whereas most of the electric field is located in the organic layer. Although the amorphous silicon layer is only 60 nm thick, the electric field is about 2×10^6 V/m. However, fully inorganic a-Si:H *nip* devices with a 300 nm intrinsic layer need electric field strength exceeding 3×10^6 V/m for sufficient charge extraction. The fields in a-Si:H and P3HT differ by a factor of 3.6 which is almost equivalent to the ratio of the dielectric constants of these materials (assuming $\epsilon = 11.9$ for a-Si:H and $\epsilon = 3.5$ for P3HT). Thus the higher polarizability of a-Si:H induces electric dipoles that screen the field in this layer stronger than in the organic material. We propose that the low electric field in the intrinsic a-Si layer in combination with undoped P3HT is the origin for the poor performance of this type of hybrid cell. As most inorganic systems have higher dielectric constants than organics, this effect might impose a general limitation to the performance of hybrid devices comprising planar interfaces oriented perpendicular to the electric field direction. Notice, that the electric field can be almost restored in the a-Si:H layer by doping the organic material. For the assumed ionized dopant concentration [24] of $5 \times 10^{17} \text{ cm}^{-3}$, the bands in the 5 wt% F4TCNQ doped P3HT layer are predicted to be almost flat, except a narrow space charge region close to the interface to the intrinsic a-Si. *In any case Fig. 4 shows that the electric field even in the doped hybrid device is lower than the one in the a-Si:H nip cell. As*

a consequence the open circuit voltage of the doped hybrid is reduced compared to the reference a-Si:H cell.

3.1 Electroabsorption

In order to support the findings from our simulations we carried out electroabsorption measurements on hybrid solar cells with undoped and doped P3HT. This technique has been applied previously to measure the distribution of the electric field in organic multilayer devices [25, 26]. For a molecular medium, application of an electric field shifts the optical transition energies via the Stark Effect.

$$\Delta E = -\Delta \vec{m} \cdot \vec{F} - \frac{1}{2} \vec{F} \circ \Delta \hat{p}_{ij} \circ \vec{F} \quad (1)$$

where \vec{F} is the electric field and $\Delta \vec{m}$ is the difference of the permanent dipole moment in the ground and excited state. $\Delta \hat{p}_{ij}$ denotes the change in the polarizability tensor upon a transition from state $|i\rangle$ to state $|j\rangle$. For a specific transition the resultant change in the absorption coefficient α due to the electric field can be mathematically expressed as a Taylor series, where higher terms can be neglected:

$$\Delta \alpha = \frac{1}{2} \Delta p \frac{d\alpha}{dE} F^2 + \frac{1}{6} (\Delta m)^2 \frac{d^2 \alpha}{dE^2} F^2 \quad (2)$$

here an isotropic distribution of dipoles was assumed:

$$\left\langle (\Delta \vec{m} \cdot \vec{F})^2 \right\rangle = \frac{1}{3} (\Delta m F)^2 \quad (3)$$

The electric field F is composed of the external applied dc and ac voltage, and the built in voltage divided by the layer thickness d :

$$F^2 = \frac{2}{d^2} [(V_{dc} - V_{bi}) V_{ac} \cos(\omega t)] + \frac{1}{2d^2} V_{ac}^2 \cos(2\omega t) + \dots \quad (4)$$

Hence an electroabsorption signal recorded at the fundamental frequency ω is proportional to the applied voltage and resembles the first or second derivative of the absorption spectrum or a superposition of them. The shape

of the signal depends on the strength of permanent and induced dipole moments in the sample. In organic materials the first derivative is more frequently observed than the second derivative. Since the samples investigated here have non transparent metal back electrodes it was necessary to measure the electroabsorption in reflection geometry. As the 100 nm Al electrode used in this work almost entirely inhibits the transmission of light, the absorption A in the entire stack of the sample is related to the reflectivity R via: $A = 1 - R$. This leads to the following expression for the experimental electroabsorption spectrum in reflection:

$$-\frac{\Delta R}{R} \propto \Delta\alpha \quad (5)$$

Generally, changes in the absorption/reflectivity of a layer stack are caused by a field-induced change in the absorption coefficient and/or by the modulation of the optical field profile due to the *alternation* of the refractive index. While the first process dominates the electroabsorption in organic samples [27], effects due to refraction index modulations cannot be neglected in amorphous silicon. However, this contribution is usually smaller than 20 % [28].

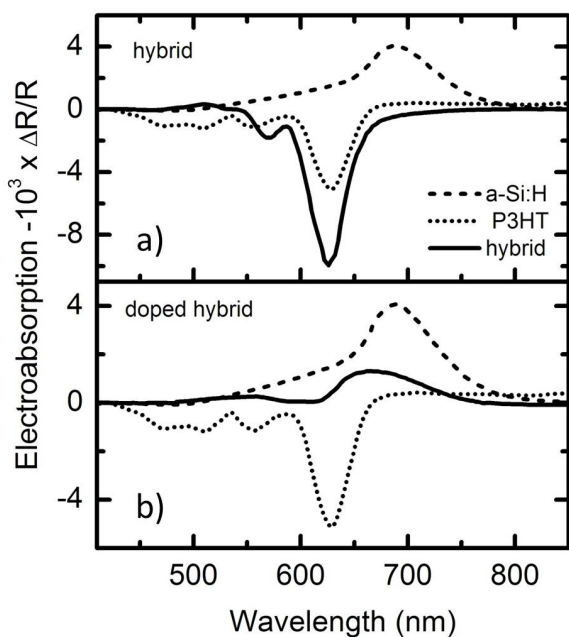


Fig. 5. a) Electroabsorption signal of ITO/a-Si:H(n,i)/P3HT/MoO₃/Al in comparison to EA-signals of the ITO/a-Si:H(n,i,p)/MoO₃/Al reference cell and a PEDOT:PSS/P3HT/Al device. The EA signal of the hybrid cell resembles the pure P3HT signal. b) The EA-signal of the doped ITO/a-Si:H(n,i)/P3HT:F4TCNQ/MoO₃/Al cell is dominated by the electroabsorption response of a-Si:H.

To analyze the electric field distribution in the hybrid cells, it was necessary to record the electroabsorption

spectra of the pure materials, a-Si:H and P3HT. As shown in Fig. 5 the EA spectrum of the a-Si cell exhibits a broad positive peak at 680 nm accompanied by a weak shoulder towards lower wavelength. The features are characteristic for amorphous silicon and can be explained by a strong contribution from the tail states to the electroabsorption signal as mentioned by Weiser *et al.* [29]. Measurements on an ITO/PEDOT:PSS/P3HT/Al structure with 60 nm active layer thickness show a strong negative derivative-like peak at 630 nm and a couple of weak side peaks at lower wavelength, which are attributed to higher transitions [30]. The P3HT signal changes its spectral shape drastically when the applied dc voltage goes from reverse to forward bias. This was attributed to the absorption by injected free charge carriers [31]. Therefore all EA signals were recorded at $V_{dc} = 4$ V in reverse bias.

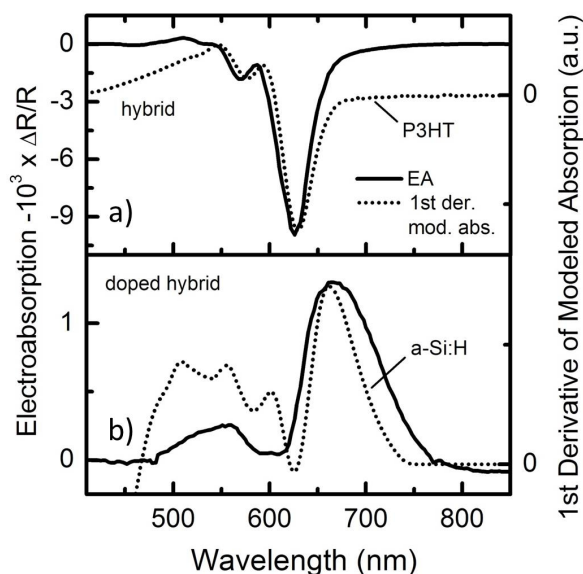


Fig. 6. a) Electroabsorption signal of ITO/a-Si:H(n,i)/P3HT/MoO₃/Al in comparison to the modeled 1st derivative absorption spectrum of P3HT in the hybrid structure. b) EA signal of the ITO/a-Si:H(n,i)/P3HT:F4TCNQ/MoO₃/Al device in comparison to the modeled 1st derivative absorption spectrum of a-Si:H in the hybrid structure.

The EA spectrum recorded for the undoped hybrid cell (Fig. 5a) is clearly dominated by the P3HT component while no contribution from the amorphous silicon can be detected. To show this more clearly, we have calculated as a function of wavelength the fraction of incident light that is absorbed in the P3HT layer, $A_{P3HT}(\lambda)$, in the actual hybrid stack. Note that the reflective back electrode leads to a standing optical wave in the stack, with the position of the minima and maxima depending on wavelength. Because

of this, the wavelength dependent absorption of the polymer in the stack is different than for the same layer on a transparent substrate without top electrode. We find an excellent correlation of the measured EA-signal with the 1st derivative of the modeled $A_{P3HT}(\lambda)$ in the stack (Fig. 6a). Since the EA-signal is directly proportional to the electric field in the corresponding layer via eq.(2) this finding confirms experimentally that most of the electrical potential drops across the undoped P3HT and, therefore, the electric field in the intrinsic a-Si layer is quite low. In contrast, the EA-signal of the hybrid cell with doped P3HT shown in Fig. 5b resembles strongly the amorphous silicon signal with an additional dip at 610 nm. As illustrated in Fig. 6b) this feature can be reproduced by the first derivative of the simulated absorption spectrum of the intrinsic a-Si:H layer, which suggests that this dip is an interference effect. However, a superposition of a weak P3HT EA-signal with the a-Si:H signal would have the same effect on the line-shape. Thus the strength of the remaining electric field in the doped P3HT might not be zero, but it is probably rather low.

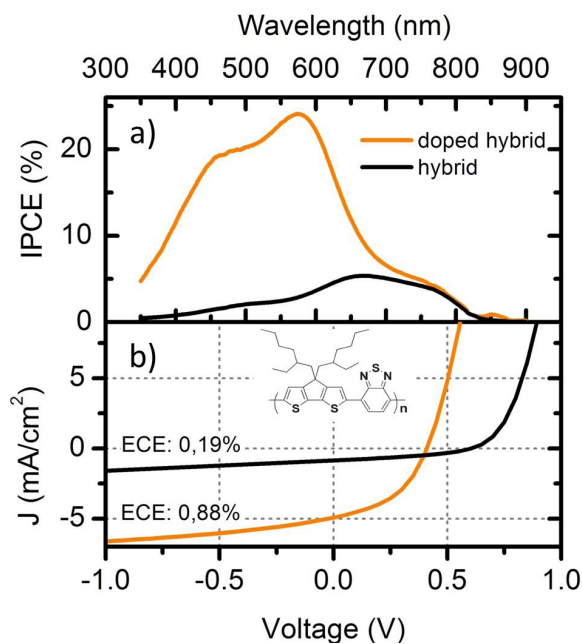


Fig. 7. a) IPCE of a hybrid cell composed of ITO/a-Si:H(n,i)/PCPDTBT/MoO₃/Al compared to the same layer system with 5 wt% PCPDTBT:F4TCNQ. b) J-V-characteristics of the hybrid cells in a).

The EA experiments confirm that the electric field across the intrinsic a-Si layer in the hybrid device with undoped P3HT is very low and that it is at least partially restored upon doping of the polymer. Similar results were found when P3HT was replaced by other organic mate-

rials, for example the small molecule zinc phthalocyanine (ZnPc) or the low bandgap polymer PCPDTBT. In both cases, hybrid solar cells with pristine organic materials showed efficiencies below 0.5 % whereas doping led to much better performances. Fig. 7 shows the effect of doping PCPDTBT in a ITO/a-Si:H(n,i)/PCPDTBT/MoO₃/Al hybrid cell, where the thickness of the PCPDTBT layer was 35 nm. The undoped hybrid device shows significant contribution from PCPDTBT to the quantum efficiency (Fig. 7a)) in the red part of the IPCE spectrum. Nevertheless the energy conversion efficiency is low due to a weak photocurrent as shown in Fig. 7b). Doping of PCPDTBT with 5 wt% F4TCNQ strongly enhances the current and the contribution from a-Si:H (blue part of the IPCE spectrum) to the quantum efficiency spectrum. In contrast to P3HT, the weak shoulder in the red part of the IPCE from 700 nm to 800 nm indicates that the polymer contributes weakly to the photocurrent in the hybrid device with doped PCPDTBT.

Table 2. Solar cell parameters of an optimized hybrid cell with 20 nm P3HT:F4TCNQ layer

material	$V_{oc}(V)$	$J_{sc}(\frac{mA}{cm^2})$	$\eta(\%)$	FF (%)
a-Si:H/P3HT:F4TCNQ	0.77	6.26	2.84	57.7

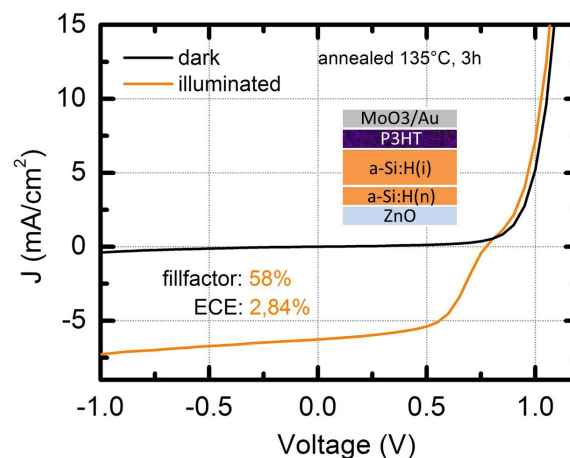


Fig. 8. J-V-characteristics of an optimized hybrid cell with 20 nm P3HT:F4TCNQ layer

Following the approach of using doped organic layers, an optimized hybrid cell was designed. Figure 8 shows the IV-characteristics of this device yielding an ECE of $\eta=2.8\%$. The solar cell characteristics are summarized in Table 2. It contained an aluminium doped ZnO layer as

the electron-collecting contact, where the workfunction of ≈ 4 eV is much smaller than that of ITO ≈ 4.7 eV, reducing the offset to the a-Si:H conduction band. Also, a very thin microcrystalline silicon layer was added between ZnO and a-Si:H which improves the contact of the n-type a-Si:H layer to the ZnO electrode. Al was replaced by Au in the back contact. The thickness of the F4TCNQ doped P3HT layer was reduced to 20 nm, which is sufficient for a hole transporting layer. The thicknesses of all other layers was the same as in the non-optimized device described above. A significant enhancement of the device performance could be achieved by annealing the complete device structure for 3h at 135°C. A priori, annealing can have different effects on the multi layer structure of the hybrid cell. One of these effects is the reduction of defect states at the inorganic/organic interface, which could lead to a better charge transfer across this junction. A second possibility is that, for the same reason, the contact to the MoO₃/Au hole-collecting electrode is improved. To keep track on this we annealed one of the samples prior to the deposition of the top electrodes. Since this treatment had no effect on the device performance we can conclude that an improved interface between the organic and the MoO₃/Au electrode causes the increased performance upon annealing. As the inorganic a-Si stack of the optimized device sample has been exposed to air considerably longer as the samples discussed previously, we attribute the slight s-shape in the current-voltage curve to the formation of an oxide barrier between a-Si:H and P3HT. Further progress shall be achieved by adjusting the band offset at the a-Si:H/organic interface by using an organic material with appropriate energy levels. A low offset between the valence band of a-Si:H and the organic HOMO enhances hole transfer from a-Si:H to the organic hole transport layer. In the same way a large offset between the conduction band of a-Si:H and the LUMO of the organic could be used as electron blocking barrier. A disadvantage in inorganic *pin* a-Si:H solar cells is the parasitic absorption of the p- and n-type transport layers. However, the bandgap of organic transport layers can be engineered in a way that the material absorbs in a spectral region complementary to that of the amorphous silicon, for example in the ultraviolet region, avoiding any parasitic absorption.

4 Conclusions

We have investigated the processes controlling the efficiency of hybrid planar devices comprising two semiconducting donor polymers and amorphous silicon. We show

that hybrid cells with an undoped polymer layer suffer from an unfavorable electric field distribution within the device, which inhibits efficient collection of charges generated in the inorganic film. This effect is shown to originate from the large difference in the dielectric constants between the inorganic and the organic layer, which causes a substantial discontinuity of the electric field across the heterojunction. We propose that this effect is quite general for hybrid two-layer devices comprising a high- ϵ inorganic semiconductor and a low- ϵ organic semiconductor, and with the hybrid heterojunction oriented perpendicular to the electric field direction. We show that one solution to this problem is doping the organic semiconductor, which restores the electric field in the amorphous silicon and enhances the performance of the device. Our results also suggest that the combination of organic and inorganic components in an interpenetrating donor-acceptor geometry, having the hybrid interface oriented mainly parallel to the electric field, shall be more efficient not only because of the larger hybrid surface area but also because of a more favorable electric field distribution within the active layer.

Acknowledgement: This work was supported by the Federal Ministry of Education and Research (BMBF) and the state government of Berlin (SENBF) in the framework of the program "Ausbau PVcomB, Spitzenforschung und Innovation in den Neuen Ländern" (grant no. 03IS2151). The authors would like to thank Thomas J.K. Brenner for additional comments to the manuscript.

References

- [1] G. Li, R. Zhu, and Y. Yang, *Nature Photonics* 6, 153 (2012).
- [2] P. J. Alet, S. Palacin, P. R. I. Cabarrocas, B. Kalache, M. Firon, and R. de Bettignies, *European Physical Journal-Applied Physics* 36, 231 (2006).
- [3] V. Gowrishankar, S. R. Scully, M. D. McGehee, Q. Wang, and H. M. Branz, *Applied Physics Letters* 89, 3 (2006).
- [4] E. L. Williams, G. E. Jabbour, Q. Wang, S. E. Shaheen, D. S. Ginley, and E. A. Schiff, *Applied Physics Letters* 87, 3 (2005).
- [5] J. H. Seo, D. H. Kim, S. H. Kwon, M. Song, M. S. Choi, R. S. Y., H. W. Lee, Y. C. Park, J. D. Kwon, K. S. Nam, Y. Jeong, J. W. Kang, and C. S. Kim, *Advanced Materials* 24, 4523 (2012).
- [6] K. Kim, J. Liu, M. A. G. Namboothiry, and D. L. Carroll, *Applied Physics Letters* 90, 3 (2007).
- [7] C. H. Chao, C. H. Chan, F. C. Wu, J. J. Huang, S. Y. Lien, K. W. Weng, and H. L. Cheng, *Solar Energy Materials and Solar Cells* 95, 2407 (2011).
- [8] R. A. Street, *Hydrogenated Amorphous Silicon*, Cambridge University Press, Cambridge, 1 edition, 1991.
- [9] M. Morana, M. Wegscheider, A. Bonanni, N. Kopidakis, S. Shaheen, M. Scharber, Z. Zhu, D. Waller, R. Gaudiana, and

- C. Brabec, *Adv. Func. Mater.* 18, 1757 (2008).
- [10] I. Lange, J. C. Blakesley, J. Frisch, A. Vollmer, N. Koch, and D. Neher, *Physical Review Letters* 106, 4 (2011).
- [11] R. Stangl, C. Leendertz, and J. Haschke, *Solar Energy* (RD Rugescu, ed.), INTECH, Croatia, 319 (2010).
- [12] S. Albrecht, W. Schindler, J. Kurpiers, J. Kniepert, J. C. Blakesley, I. Dumsch, S. Allard, K. Fostiropoulos, U. Scherf, and D. Neher, *Journal of Physical Chemistry Letters* 3, 640 (2012).
- [13] D. Mühlbacher, M. Scharber, M. Morana, Z. Zhu, D. Waller, R. Gaudiana, and C. J. Brabec, *Advanced Materials* 18, 2884 (2006).
- [14] K. F. Jeltsch, M. Schädel, J. B. Bonekamp, P. Niyamakom, F. Rauscher, H. W. A. Lademann, I. Dumsch, S. Allard, U. Scherf, and K. Meerholz, *Adv. Funct. Mater.* 22, 397 (2012).
- [15] Z. Zhu, D. Waller, R. Gaudiana, M. Morana, D. Mühlbacher, M. Scharber, and C. J. Brabec, *Macromolecules* 40, 1981 (2007).
- [16] G. F. Burkhard, E. T. Hoke, and M. D. McGehee, *Advanced Materials* 22, 3293 (2010).
- [17] L. A. A. Pettersson, L. S. Roman, and O. Inganäs, *Journal of Applied Physics* 86, 487 (1999).
- [18] F. C. Spano, J. Clark, C. Silva, and R. H. Friend, *Journal of Chemical Physics* 130, 16 (2009).
- [19] C. Tanase, E. J. Meijer, P. W. M. Blom, and D. M. de Leeuw, *Physical Review Letters* 91, 4 (2003).
- [20] Y. A. Zhang and P. W. M. Blom, *Applied Physics Letters* 97, 3 (2010).
- [21] I. Salzmänn, G. Heimel, S. Duhm, M. Oehzelt, P. Pingel, B. M. George, A. Schnegg, K. Lips, R. P. Blum, A. Vollmer, and N. Koch, *Physical Review Letters* 108, 035502 (2012).
- [22] R. Stangl, M. Kriegel, S. Kirste, M. Schmidt, and W. Fuhs, *Proc. IEEE-31, 31th IEEE Photovoltaics Specialists Conference, Orlando, USA (January 2005)*.
- [23] L. Korte and M. Schmidt, *Journal of Non-Crystalline Solids* 354, 2138 (2008).
- [24] P. Pingel, R. Schwarzl, and D. Neher, *Applied Physics Letters* 100, 143303 (2012).
- [25] P. A. Lane, J. Rostalski, C. Giebeler, S. J. Martin, D. D. C. Bradley, and D. Meissner, *Solar Energy Materials and Solar Cells* 63, 3 (2000).
- [26] M. C. Gather, R. Jin, J. de Mello, D. D. C. Bradley, and K. Meerholz, *Applied Physics B* 95, 113 (2009).
- [27] I. H. Campbell, J. P. Ferraris, T. W. Hagler, M. D. Joswick, I. D. Parker, and D. L. Smith, *Polymers for Advanced Technologies* 8, 417 (1997).
- [28] J. H. Lyou and E. A. Schiff, *Review of Scientific Instruments* 75, 921 (2004).
- [29] G. Weiser, U. Dersch, and P. Thomas, *Philosophical Magazine B-Physics of Condensed Matter Statistical Mechanics Electronic Optical and Magnetic Properties* 57, 721 (1988).
- [30] R. Österbacka, C. P. An, X. M. Jiang, and Z. V. Vardeny, *Science* 287, 839 (2000).
- [31] P. J. Brown, H. Sirringhaus, and R. H. Friend, *Synthetic Metals* 101, 557 (1999).

Received August 16, 2013; accepted January 10, 2014.